PERGAMON

Mechanism and Machine Theory 35 (2000) 1257–1267

MECHANISM AND MACHINE THEORY

www.elsevier.com/locate/mechmt

Optimum design of 3-DOF spherical parallel manipulators with respect to the conditioning and stiffness indices

Xin-Jun Liu[a,*], Zhen-Lin Jin[b], Feng Gao[c]

[a]*Manufacturing Engineering Institute, Department of Precision Instruments, Tsinghua University, Beijing, 100084 People's Republic of China*

[b]*Robotic Research Center, Yanshan University, Qinhuangdao, Hebei, People's Republic of China, 066004*

[c]*Robotics Research Center, Hebei University of Technology, Tianjin, People's Republic of China, 300130*

Received 07 December 1998; accepted 02 September 1999

Abstract

This paper concerns the use of evaluation criteria, such as, the conditioning index, the stiffness to select the link lengths of 3-DOF spherical parallel manipulators (3-DOF SPMs) and analyze their operational performance. The atlases of the global conditioning index and the global stiffness index are obtained in the solution space to optimize the link lengths of 3-DOF SPMs; the dexterity and stiffness maps of the manipulators are presented to analyze the operational performance, from which we can see that the global or local conditioning index is identical with global or local stiffness index. A method for obtaining these maps for 3-DOF SPMs is presented. The maps will reveal the existence of zones where the stiffness is not acceptable and will also help the designer by proving a more accurate representation of the properties of the manipulator. The technique has wide application in the design of the serial and parallel robots. © 2000 Elsevier Science Ltd. All rights reserved.

1. Introduction

Robotic mechanism optimum design can be based on the use of evaluation criteria involving workspace [1,2], dexterity [3,4], payload [5], global conditioning index [6,7], and stiffness [8]. Among these properties of mechanical systems, the latter two are particularly important in the context of parallel manipulators. According to the analysis of Gosselin [9,10], there are three

* Corresponding author..
E-mail address: xjliu@ysu.edu.cn (X.-J. Liu).

0094-114X/00/$ - see front matter © 2000 Elsevier Science Ltd. All rights reserved.
PII: S0094-114X(99)00072-5

types of singularities for parallel manipulators which make them different from the serial ones. These types of singularities correspond to configurations for which there exists a certain set of nonzero generalized velocity vectors of the gripper link that produce a velocity of zero at all the actuators. Therefore, the motion of the gripper link cannot be controlled by the motion of the actuators, and the condition number of the Jacobian matrix and the stiffness of the manipulator will go to zero.

The condition number of Jacobian matrix of the manipulator has attracted the attention of some researchers [11,12]. In fact, the condition number of a matrix is used in numerical analysis to estimate the error generated in the solution of a linear system of equations by the error on the data [13]. When applied to the Jacobian matrix, the condition number will give a measure of the accuracy of the Cartesian velocity of the end effector and the static load acting on the end effector. Indeed, as shown by Salisbury and Craig [14], the dexterity of a manipulator can be defined as the condition number of its Jacobian matrix. Gosselin applied the dexterity based on the condition number of the Jacobian matrix to the optimization of planar and spatial manipulators [4]. The condition number has already been used for the kinematic design of 3-DOF planar parallel manipulators [15] and 3-DOF spherical parallel manipulators [16]. The global conditioning index (GCI) was defined and applied to the optimization of robotic manipulators [12]. The atlases of GCI for 2-DOF planar parallel manipulators are obtained to optimize the manipulators [6,7].

Although some methods and criteria have been developed for the design of robotic mechanisms, and many types of robotic mechanisms have been proposed, there has not been a unified method for the design. One reason for this is that it is difficult to identify which group of link length is optimum in the context of performance criteria of the manipulators. Therefore, it is of primary importance to develop some useful tools that will allow us to understand the relationships between the criteria and link lengths of the manipulators. From papers [17–19] we can see that the solution space of manipulators is a useful one. It can be used to study various performances of robotic mechanisms, and is a useful tool for the designer to select optimum manipulators.

In this paper, the condition number is applied to the Jacobian matrix and the stiffness matrix of 3-DOF SPMs. The atlases of GCI and global stiffness index (GSI) are obtained in the solution space established in the paper [20], which are used to optimize the link lengths of 3-DOF SPMs. The local dexterity and stiffness maps plotted in the reachable workspace can be used to study the dexterity and stiffness of the 3-DOF SPM. The results show that the atlases (or maps) of GCI (or local dexterity) are identical to those of GSI (or local stiffness). The technique used in this paper can be applied to the optimization of other serial or parallel manipulators.

2. The solution space of 3-DOF SPMs

The special geometry of spherical mechanisms, such as 3-DOF SPMs, occurs when all joint axes intersect at a common point, referred to the center of the manipulator. The 3-DOF SPM is composed of two ternary links as shown in Fig. 1, one of which is considered the fixed link and the other the moving link. The lower ternary link is the fixed link, while the upper ternary

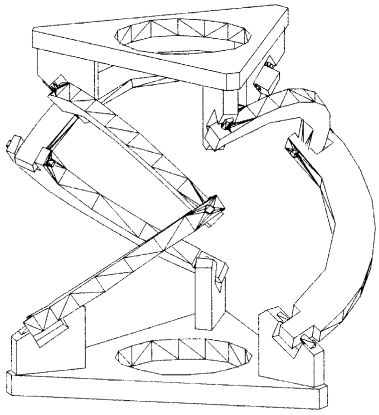

Fig. 1. The general architecture of a 3-DOF SPMs.

is the moving link which has three degrees-of-freedom spherical motion relative to the fixed one.

Since the manipulator should be symmetric, the geometric parameters of a 3-DOF SPM can be reduced to four angles α_1, α_2, β_1 and β_2 as shown in Fig. 2 and [20]

$$\begin{cases} 0 \le \beta_1 \le 90^\circ \\ 0 < \beta_2 \le 90^\circ \\ 0 \le \alpha_1, \alpha_2 \le 180^\circ \end{cases} \tag{1}$$

and

$$\begin{cases} \alpha_1 + \alpha_2 + \beta;_2 > \beta_1 \\ \alpha_1 > \alpha_2 + \beta_3 \text{ and } \alpha_1 - (\alpha_1 + \beta_2) < 180^\circ - \beta_1 \\ \alpha_2 > \alpha_1 + \beta_2 \text{ and } \alpha_2 - (\alpha_1 + \beta_2) < 180^\circ - \beta_1 \end{cases} \tag{2}$$

from which we can obtain the solution space of 3-DOF SPMs, which is the polyhedron ABCDEFGHIJKLMN as shown in Fig. 3. When $\beta_2 = a$ $(0 < a \ll 90^\circ)$, it is a polygon paralleling to the plane $0 - \alpha_1\alpha_2$ [20].

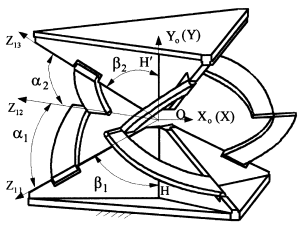

Fig. 2. Geometric parameters of the 3-DOF SPMs.

3. The Jacobian and stiffness matrices of 3-DOF SPMs

The Jacobian matrix is defined as the matrix map of the angular velocity of the end effector into the vector of actuated joint rates. Indeed, we have

$$\dot{\boldsymbol{\theta}} = \mathbf{J}\boldsymbol{\omega} \tag{3}$$

where $\dot{\boldsymbol{\theta}}$ is the vector of actuated joint rates and $\boldsymbol{\omega}$ is the vector giving the angular velocity of the end effector. From Gosselin and Angeles [10], we have, for parallel chains, the following equation:

$$\mathbf{A}\boldsymbol{\omega} + \mathbf{B}\dot{\boldsymbol{\theta}} = 0 \tag{4}$$

which leads to

$$\mathbf{J} = -\mathbf{B}^{-1}\mathbf{A} \tag{5}$$

For 3-DOF SPMs, matrices **A** and **B** are given in Gosselin and Angeles [10], and can be written as

$$\mathbf{A} = \begin{bmatrix} (\boldsymbol{w}_1 \times \boldsymbol{v}_1)^{\mathrm{T}} \\ (\boldsymbol{w}_2 \times \boldsymbol{v}_2)^{\mathrm{T}} \\ (\boldsymbol{w}_3 \times \boldsymbol{v}_3)^{\mathrm{T}} \end{bmatrix} \tag{6}$$

and

$$\mathbf{B} = \mathrm{diag}\,(\boldsymbol{w}_1 \times \boldsymbol{u}_1 \cdot \boldsymbol{v}_1, \boldsymbol{w}_2 x \times \boldsymbol{u}_2 \cdot \boldsymbol{v}, \boldsymbol{w}_3 \times \boldsymbol{u}_3 \cdot \boldsymbol{v}_3) \tag{7}$$

where, $\boldsymbol{w}_i$, $\boldsymbol{u}_i$, $\boldsymbol{v}_i$ ($i = 1, 2, 3$) are the vectors along the axes of revolute joints as shown in Fig. 2.

By virtue of what is called the *duality of kinematic and static* [21], the forces and moments applied at the gripper under static conditions are related to the forces or moments required at the actuators to maintain the equilibrium by the transpose of the Jacobian matrix **J**. We can write

$$\boldsymbol{\tau} = \mathbf{J}^{\mathrm{T}}\boldsymbol{f} \tag{8}$$

where $\boldsymbol{f}$ is the vector of actuator forces or torques, and $\boldsymbol{\tau}$ is the generalized vector of Cartesian forces and torques at the end effector. The stiffness matrix is then given [22] as the following

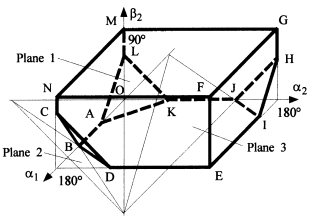

Fig. 3. The solution space for 3-DOF SPMs.

$$\mathbf{K} = k\mathbf{J}^{\mathrm{T}}\mathbf{J} \tag{9}$$

where k is a scalar representing the stiffness of each of the actuators. The factor k can be omitted since it acts as a scaling factor on matrix $\mathbf{K}$. Let $k = 1$, we can obtain another expression of stiffness matrix as the following

$$\mathbf{C} = \mathbf{J}^{\mathrm{T}}\mathbf{J} \tag{10}$$

Hence, the stiffness matrix of the 3-DOF SPM can be computed from the expression of Jacobian matrix.

4. Atlases of the GCI and the GSI of 3-DOF SPMs

4.1. The GCI and GSI

As shown by Strang [13], the condition number of a matrix is used in numerical analysis to estimate the error generated in the solution of a linear system of equations by the error on the data. When applied to the Jacobian matrix, the condition number will give a measure of the accuracy of the Cartesian velocity of the end effector and the static load acting on the end effector. It can also be used to evaluate the dexterity of a manipulator [14]. The condition number of Jacobian matrix can be written as

$$\kappa_{\mathrm{J}} = \|\mathbf{J}\| \, \|\mathbf{J}^{-1}\| \tag{11}$$

where $\|\cdot\|$ denotes any norm of its matrix argument. In this paper, the following frame-invariant norm is adopted throughout:

$$\|\mathbf{J}\| = \sqrt{tr\left(\mathbf{J}\boldsymbol{W}\mathbf{J}^{\mathrm{T}}\right)} \tag{12}$$

where $\boldsymbol{W}$ is defined as $w\mathbf{1}$ and $w = 1/n$, n is the dimension of the square matrix $\mathbf{J}$.

The global conditioning index (GCI) η_{J} is defined as the inverse of the condition number of the Jacobian matrix integrated over the reachable workspace and divided by the volume of the workspace. Therefore, η_{J} can be written as

$$\eta_{\mathrm{J}} = \frac{\int_W (1/\kappa_{\mathrm{J}}) \, \mathrm{d}W}{\int_W \mathrm{d}W} \tag{13}$$

which is used to measure the global behavior of the manipulator condition number, and W is the manipulator's reachable workspace.

Similarly, the global stiffness index (GSI) η_{C} is the inverse of the condition number of the stiffness matrix integrated over the reachable workspace and divided by the volume of the workspace. Therefore, the condition number of stiffness matrix and GSI η_{C} can be easily written as

$$\kappa_C = \|\boldsymbol{C}\|\|\boldsymbol{C}^{-1}\| \tag{14}$$

and

$$\eta_C = \frac{\int_W (1/\kappa_C)\, dW}{\int_W dW} \tag{15}$$

which are used to evaluate the local and global stiffness of the manipulator, respectively.

4.2. Atlases of the GCI and GSI

The reachable workspace for 3-DOF SPMs is systematically studied in papers [20]. From Eqs. (11), (13)–(15), we can calculate η_J and η_C of all manipulators in the solution space, given the parameters β_1 and β_2. And we can obtain the atlases of GCI η_J as shown in Fig. 4(a)–(l). Some atlases of GSI η_C are shown in Fig. 5(a)–(c). From Fig. 4(a)–(l) and Fig. 5(a)–(c), we can see that:

- The atlases of the GCI are identical to those of the GSI, except for that the value of η_J is larger than that of η_C. Therefore, from atlases of GCI (for example Fig. 4(a)–(l)), we can also understand the distribution of GSI in the solution space.
- From Fig. 4(a)–(c), we can see that the GCI is symmetric about lines $\alpha_1 = 90^\circ$ and $\alpha_2 = 90^\circ$ in the solution space when $\beta_1 = 0^\circ$.
- From Fig. 4(f), (i)–(l), we can see that the GCI is symmetric about lines $\alpha_1 = 90^\circ$ in the solution space when $\beta_1 = 90^\circ$ or $\beta_2 = 90^\circ$
- When $\alpha_1 = 90^\circ$ and $\alpha_2 = 90^\circ$, values of the GCI and GSI for manipulators in all atlases are larger than that of other manipulators. Therefore, the GCI and GSI of the manipulators are better.
- From Fig. 4(a)–(l), we optimize the three 3-DOF SPMs as shown in Table 1.

Table 1
Examples optimized using the technique described in Section 4

Geometrical parameters of 3-DOF SPMs				Global conditioning index
α_1	α_2	β_1	β_2	
90deg;	90deg;	60deg;	45deg;	0.58
90deg;	90deg;	60deg;	60deg;	0.61
90deg;	90deg;	60deg;	90deg;	0.65

5. Dexterity and stiffness maps of 3-DOF SPMs

In Section 4, we optimize 3-DOF SPMs using the global conditioning index and global stiffness index in the solution space. In this section, the condition numbers of Jacobian matrix and stiffness matrix described in Section 4 will be used to obtain dexterity and stiffness maps

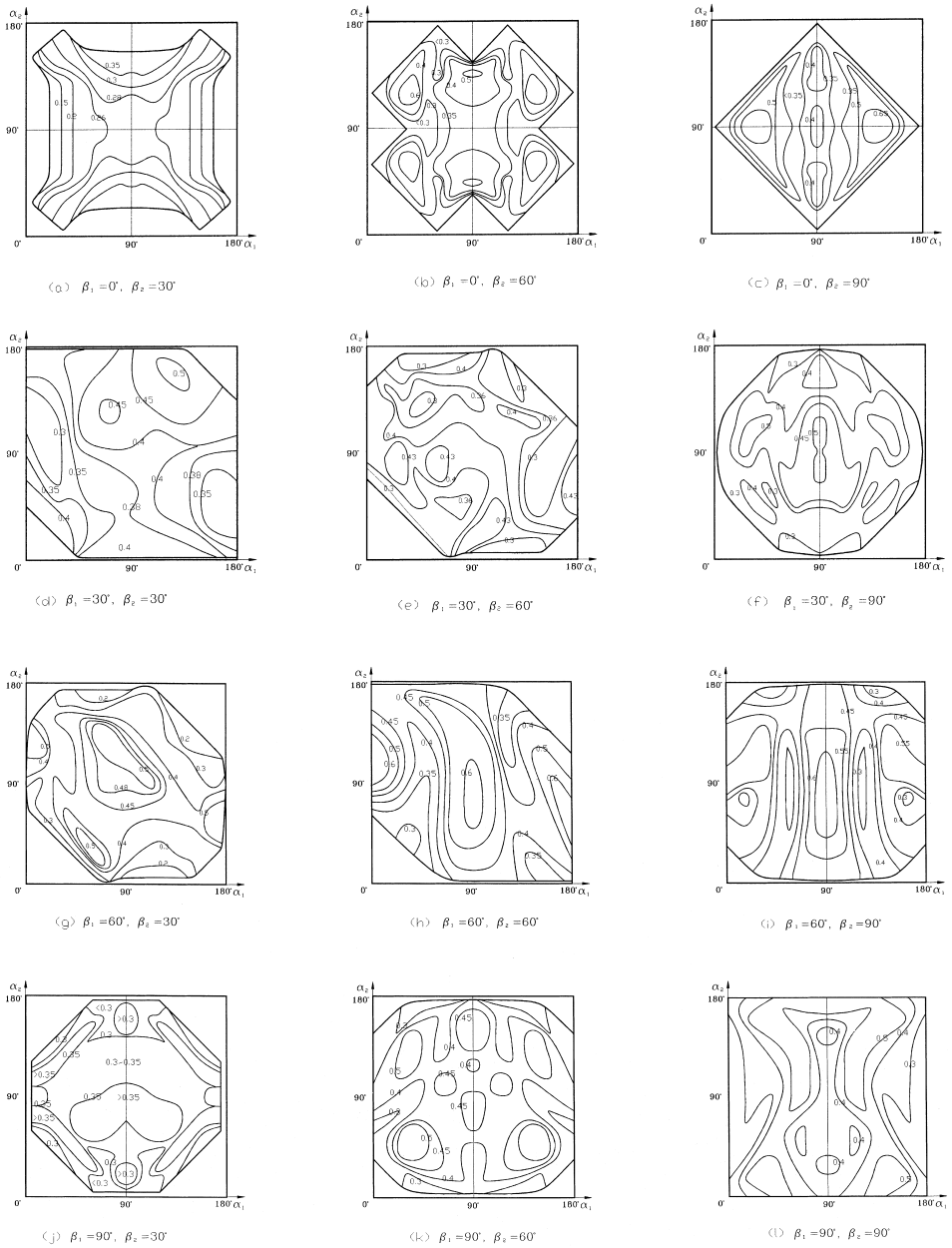

Fig. 4. The atlases of GCI for 3-DOF SPMs.

for 3-DOF SPMs. The maps are drawn on the reachable workspace on the Conformal Transformation Plane [20]. Therefore, the determination and the plane figure of the workspace for 3-DOF SPMs described in [20] will be adopted here.

5.1. The local conditioning index (LCI) and local stiffness index (LSI) of 3-DOF SPMs

From the paper [20], we know that the orientation and direction of the end effector of the 3-DOF SPM can be specified by a rotation matrix **Q**, which can be represented by three Euler angles noted ϕ_1, ϕ_1 and ϕ_1, respectively. The matrix **Q** (the rotation from frame O-$X_0Y_0Z_0$ to frame O-XYZ as shown in Fig. 2) is written as

$$\mathbf{Q} = \begin{bmatrix} q_{11} & q_{12} & q_{13} \\ q_{21} & q_{22} & q_{23} \\ q_{31} & q_{32} & q_{33} \end{bmatrix} \tag{16}$$

where

$$\begin{aligned} q_{11} &= -sin\ \phi_1\ sin\ \phi_3 + cos\ \phi_1\ cos\ \phi_3\ cos\ \phi_2 \\ q_{12} &= -sin\ \phi_1\ cos\ \phi_3 - cos\ \phi_1\ sin\ \phi_3\ cos\ \phi_2 \\ q_{13} &= cos\ \phi_1\ sin\ \phi_2 \\ q_{21} &= cos\ \phi_1\ sin\ \phi_3 + sin\ \phi_1\ sin\ \phi_3\ cos\ \phi_2 \\ q_{22} &= cos\ \phi_1\ cos\ \phi_3 - sin\ \phi_1\ sin\ \phi_3\ cos\ \phi_2 \\ q_{23} &= sin\ \phi_1\ sin\ \phi_2 \\ q_{31} &= -cos\ \phi_3\ sin\ \phi_2 \\ q_{32} &= sin\ \phi_3\ sin\ \phi_2 \\ q_{33} &= cos\ \phi_2 \end{aligned} \tag{17}$$

If the Z–Y–Z rotation (ϕ_1–ϕ_2–ϕ_3) is applied to the matrix **Q**, the orientation of the end effector is specified by the vector $(q_{13}, q_{23}, q_{33})^T$, which means that two Euler angles ϕ_1 and ϕ_1 determine the orientation of the effector.

From Eqs. (11) and (14), we can see that the condition numbers (κ_J and κ_C) of Jacobian and stiffness matrices are dependent on the orientation and direction (ϕ_1, ϕ_2 and ϕ_3) of the end effector of the manipulator. Given one point on the workspace, the orientation (ϕ_1 and ϕ_1) of the end effector can be known and the condition number is of dependence on the direction (ϕ_3)

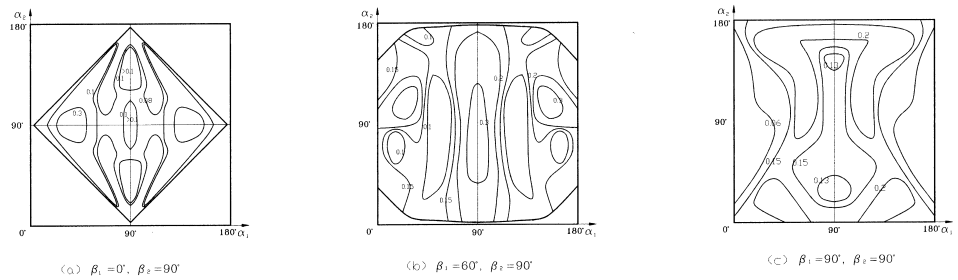

Fig. 5. The atlases of GSI for 3-DOF SPMs.

of the end effector. Therefore, we define the local conditioning index (LCI) ζ_J and local stiffness index (LSI) ζ_C as

$$\zeta_J = \frac{\int_{\phi_3} (1/\kappa_J)\, d\phi_3}{\int_{\phi_3} d\phi_3} \tag{18}$$

$$\zeta_C = \frac{\int_{\phi_3} (1/\kappa_C)\, d\phi_3}{\int_{\phi_3} d\phi_3} \tag{19}$$

where $0 < \zeta_J \leq 1$ and $0 < \zeta_C \leq 1$.

5.2. Dexterity and stiffness maps

From Eqs. (18) and (19), the LCI and LSI of the 3-DOF SPMs can be calculated. The maps of the LCI and LSI can be obtained on the reachable workspace of the 3-DOF SPM on the Conformal Transformation Plane, which are called dexterity and stiffness maps, respectively. The technique is illustrated by three 3-DOF SPMs optimized in Section 4, the reachable workspace of each of which is presented as the whole surface of a sphere [20]. The dexterity and stiffness maps are shown in Figs. 6 and 7, respectively. In Figs. 6 and 7, we can see that

- The dexterity and stiffness are larger near the center of the workspace of upper circle plane on the Conformal Transformation Plane. This is in accordance with what would be intuitively expected.
- Since the manipulator is symmetric, the dexterity and stiffness are symmetric too, which can be seen from Fig. 6(a)–(c) present diagrams identical to the ones of Fig. 7(a)–(c) but for that the value of ζ_C is larger than that of ζ_J. Therefore, from maps of LCI, we can also understand the distribution of LSI.

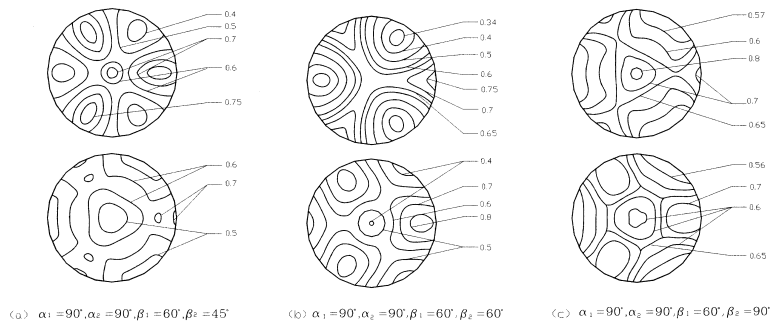

Fig. 6. Dexlerity maps of 3–DOF SPMs.

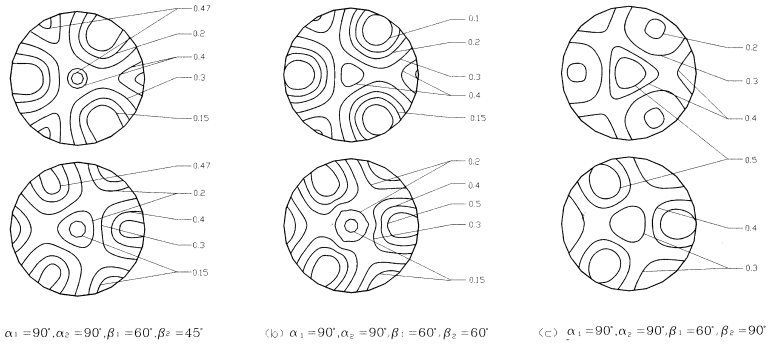

(a) $\alpha_1 = 90°, \alpha_2 = 90°, \beta_1 = 60°, \beta_2 = 45°$ (b) $\alpha_1 = 90°, \alpha_2 = 90°, \beta_1 = 60°, \beta_2 = 60°$ (c) $\alpha_1 = 90°, \alpha_2 = 90°, \beta_1 = 60°, \beta_2 = 90°$

Fig. 7. Stiffness maps of 3–DOF SPMs

6. Conclusion

The problem of the computer-aided kinematic design of 3-DOF SPMs has been addressed in this article. It has been recalled that the concepts of dexterity and stiffness are intimately related. Then, the tools have provided the designer with the ways of optimizing the link lengths of manipulators and analyzing the dexterity and stiffness of 3-DOF SPMs on the reachable workspace. Examples of optimized 3-DOF SPMs and dexterity and stiffness maps are given and interpreted. Since the dexterity and stiffness are important issues in the context of parallel, the method can also be extended to other parallel manipulators.

References

[1] K.C. Gupta, On the nature of robot workspace, The international Journal of Robotics Research 5 (2) (1985) 112–121.
[2] C.M. Gosselin, M. Jean, Determination of the workspace of planar parallel manipulators with joint limits, Robotics and Autonomous Systems 17 (1996) 129–138.
[3] C.A. Klein, B.E. Blaho, Dexterity measures for the design and control of kinematiclly redundant manipulators, The International Journal of Robotics Research 6 (1987) 72–82.
[4] C.M. Gosselin, The optimum design of robotic manipulators using dexterity indices, Robotics and Autonomous Systems 9 (1992) 213–226.
[5] Feng Gao, Febrice Guy, W.A. Gruver, Criteria based analysis and design of three Degree-of-Freedom planar robotic manipulators, in: Proceedings of the 1997 IEEE International Conference on Robotics and Automation, New Mexico-April, 1997, pp. 468–473.
[6] Feng Gao, Xin-jun Liu, W.A. Gruver, The global conditioning index in the solution space of two Degree-of-Freedom planar parallel manipulators, in: IEEE SMC'95,Canada, 1995, pp. 4055–4058.
[7] Feng Gao, Xin-Jun Liu, W.A. Gruver, Performance evaluation of two degrees-of-freedom planar parallel robots, Mechanism and Machine Theory 33 (2) (1998) 661–668.
[8] C. Gosselin, Stiffness map for parallel manipulators, IEEE Transaction on Robotics and Automation 6 (3) (1990) 377–382.

[9] C. Gosselin, Kinematic analysis, optimization and programming of parallel robotic manipulators, PH.D. thesis, McGill University, Montréal, Québec, Canada (1988).
[10] C. Gosselin, J. Angeles, Singularity analysis of closed-loop kinematic chains, IEEE Transaction on Robotics and Automation 6 (3) (1990) 281–290.
[11] J. Angeles, C. López-Cajún, Kinematic isotropy and the conditioning index of serial robotic manipulators, Int. J. Robot. Res. 11 (6) (1992) 560–571.
[12] C. Gosselin, J. Angeles, A global performance index for the kinematic optimization of robotic manipulators, Transaction of the ASME, Journal of Mechanical Design 113 (1991) 220–226.
[13] G. Strang, Linear Algebra and its Application, Academic Press, New York, 1976.
[14] J.K. Salisbury, J.J. Graig, Articulated hands: force control and kinematic issues, The International Journal of Robotics Research 1 (1) (1982) 4–17.
[15] C. Gosselin, J. Angeles, The optimum kinematic design of a planar three-degree-of-freedom parallel manipulators, ASME J. Mechanisms, Transmissions, Automations. Design 110 (1) (1988) 35–41.
[16] C. Gosselin, J. Angeles, The optimum kinematic design of a spherical three Degree-of-Freedom parallel manipulator, J. Mech. Transm. Autom. Des. 111 (2) (1989) 202–207.
[17] Feng Gao, X.Q. Zhang, W.B. Zu, Y.S. Zhao, Distribution of some properties in a physical model os the solution space of 2-DOF parallel planar manipulators, Mechanism and Machine Theory 30 (6) (1995) 811–817.
[18] Feng Gao, X.Q. Zhang, Y.S. Zhao, H.R. Wang, A physical model of the solution space and the atlases of the reachable workspace for 2-DOF parallel planar manipulators, Mechanisms and Machine Theory 31 (2) (1996) 173–184.
[19] Feng Gao, Y.S. Zhao, Z.H. Zhan, Physical model of the solution space for 3-DOF parallel planar manipulators, Mechanisms and Machine Theory 31 (2) (1996) 161–171.
[20] Xin-Jun Liu, The relationships between the performance criteria and link lengths of the parallel manipulators and their design theory, Ph.D. thesis, Yanshan University, Qinhuangdao, China (1999). (In China).
[21] K.J. Waldron, K.H. Hunt, Series-parallel dualities in actively coordinated mechanisms, Robotics Research 4 (1988) 175–181.
[22] K.M. Lee, R. Johnson, Static characteristics of an in-parallel actuated manipulator for clamping and bracing applications, in: Proc. IEEE Int. Conf. Robotics Automat, 1989, pp. 1408–1413.